Shell model study of the neutron rich isotopes from oxygen to silicon

E. Caurier,[1] F. Nowacki,[2] A. Poves,[3] and J. Retamosa[4]
[1]*CRN IN2P3-CNRS/Université Louis Pasteur Boîte Postal 20, F-67037 Strasbourg Cedex, France*
[2]*Laboratoire de Physique Theorique, Université Louis Pasteur, 67084 Strasbourg Cedex, France*
[3]*Departamento de Física Teórica C-XI, Universidad Autónoma de Madrid, E-28049 Madrid, Spain*
[4]*Departamento de Física Atómica y Nuclear, Universidad Complutense de Madrid, E-28040 Madrid, Spain*
(Received 20 January 1998)

In this paper we extend the shell model calculations previously made for the very neutron-rich nuclei with $Z \geqslant 14$ to Al, Mg, Na, Ne, F, and O, using the same valence space and effective interaction. Predictions are made for the neutron separation energies and for the location of the neutron drip line. We find that the isotopes of Ne, Na, and Mg are deformed for $N \geqslant 22$. In ^{40}Mg, which is at the edge of the drip line, the $N=28$ shell closure does not stand. By enlarging the valence space to include intruder states we are able to account for the vanishing of the $N=20$ neutron shell closure in a small region around ^{31}Na that we delineate. The dominance of the intruders explains the collective features experimentally found in this region. [S0556-2813(98)04309-X]

PACS number(s): 21.60.Cs, 21.10.Dr, 27.30.+t, 27.40.+z

I. INTRODUCTION

In a recent article [1] we presented the results of large scale shell model calculations that describe successfully all the known isotopes of the elements with $Z=14$ up to $Z=20$. We discussed in detail their behavior at the $N=28$ neutron shell closure which was claimed to be broken in this very neutron rich regime [2]. We concluded that it was rather the case of a strongly correlated closed shell than a proper vanishing of its magicity. In this paper we extend these calculations to the lighter elements, aluminum to oxygen. We expect some of these nuclei to be deformed for $N \geqslant 22$ due to the presence of neutrons and protons in active orbits. Furthermore the deformation region may reach in some cases the drip line, whose location is also a goal of our work. Around $N=20$ another problem has to be considered; the vanishing of the $N=20$ shell closure, already well documented experimentally [3–7] and theoretically [8–13]. We will address this problem by enlarging our valence space to incorporate the intruder configurations that are responsible for the existence of an island of deformation around ^{31}Na, where semimagic nuclei were expected in the standard shell model view. The inversion of ''normal'' and intruder configurations will be seen to cause the vanishing of the $N=20$ neutron shell closure. We will delineate the borders of the region, disentangle the structure of the deformed states, and make comparisons with the existing experimental results and predictions where they are not available.

We have organized the paper as follows: First we present our results in a valence space that assumes that $N=20$ is closed. This model is shown to be valid for $N \geqslant 22$ in all cases. We compare with the data on binding energies, make predictions on the situation of the drip line, spectroscopic properties, etc. We analyze the discrepancies and point out the limitations of our approach close to $N=20$. Secondly, we enlarge the space to allow for the presence of intruder states, whose properties we study. In particular, the relative position of the normal and intruder configurations that led us to the location of the region of deformation around ^{31}Na. We include a short section devoted to ^{34}Si, that we find to resemble a doubly magic nucleus. Finally we comment on the available mean field results and close the paper with our conclusions.

II. $0\hbar\omega$ DESCRIPTION OF THE ISOTOPIC CHAINS FROM $Z=8$ UP TO $Z=13$

A. Separation energies and situation of the neutron drip line

In this section we use the valence space defined in our previous work [1], i.e., the full sd shell for Z-8 protons and the full pf shell for N-20 neutrons. We refer the reader to this paper for a more detailed description of the effective interaction whose main parts are the W Hamiltonian of Wildenthal for the sd shell [14] and the KB' interaction [15] for the pf shell. We use standard quadrupole effective charges $e_\pi = 1.5$ and $e_\nu = 0.5$. The maximum m-scheme dimension we have handled in this work is 10^7 (defined as the number of $M=0$ Slater determinants). In the calculation of the binding energies from the nuclear energies coming out of our calculation we proceed as in Ref. [1].

The one and two neutron separation energies (S_N and S_{2N}) are plotted in Figs. 1 and 2 for all the elements we are considering. It is seen that the agreement for the Al chain is excellent for all the neutron numbers. This is the kind of results that we had found for $Z>14$ in [1]. For oxygen and fluorine the data are limited to $N<20$ where our results are identical to Wildenthal's. It is for Ne, Na, and Mg that a clear anomaly appears around $N=20$, that is the fingerprint of the breaking of the shell closure, as we will discuss later. Besides, our calculation gives a $5/2^-$ ground state for ^{31}Na while experimentally it is known to be a $3/2^-$ [4]. Other experimental results that are not well reproduced in this valence space are the half-lives of the isotopes close to $N=20$ [6]. Very recently an update of these measurements and a comparison with the theoretical predictions of our model has been made in Ref. [16]. Hence we will not dwell on these aspects here.

According to our calculations the last bound isotopes are ^{24}O, ^{27}F, ^{34}Ne, ^{37}Na, ^{38}Mg, and ^{41}Al. Notice, however, that we cannot exclude slight changes on the position of the drip line, since ^{37}Na is only bound by 250 keV and ^{29}F, ^{31}F,

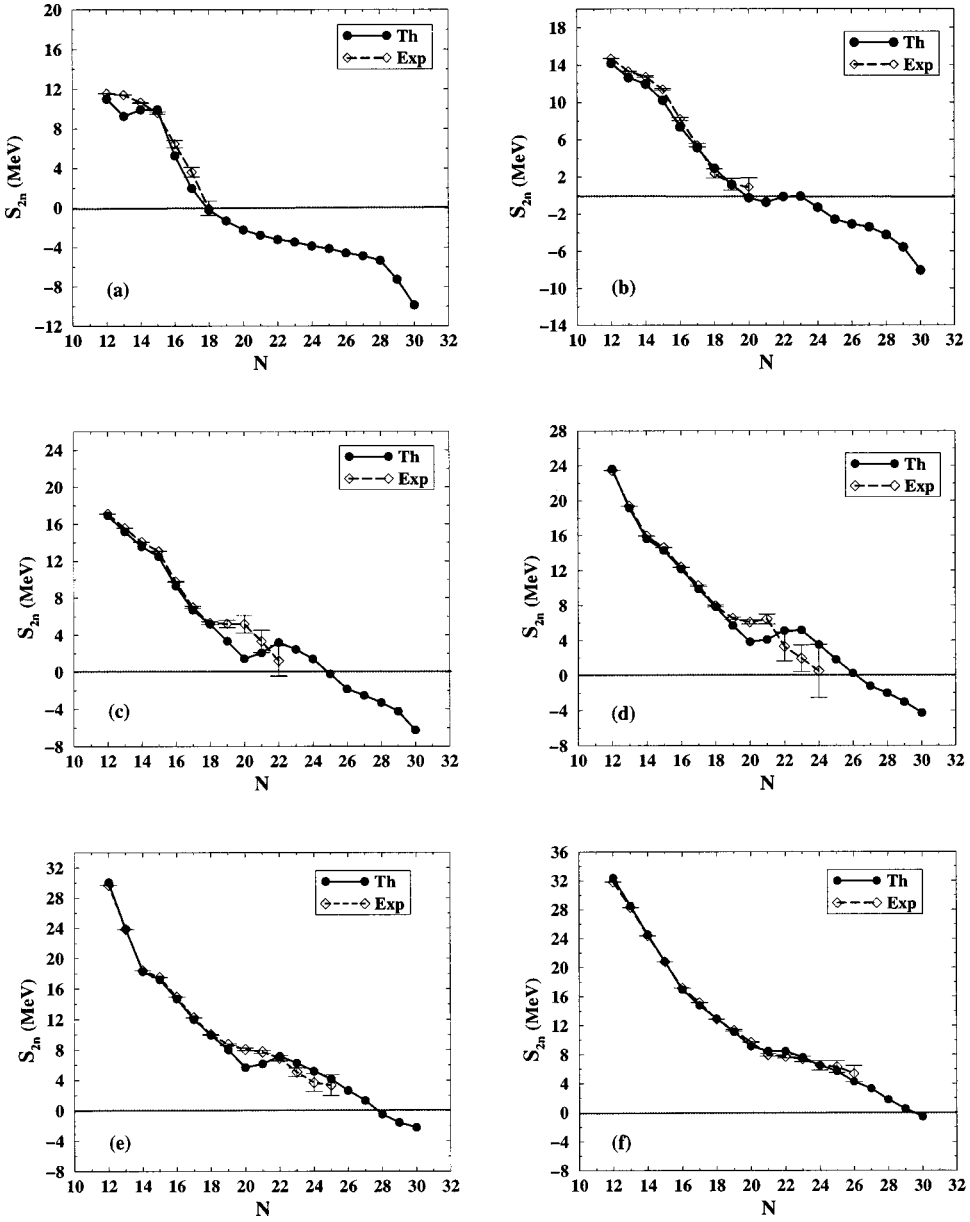

FIG. 1. Theoretical and experimental S_{2n} for O (a), F (b), Ne (c), Na (d), Mg (e), and Al (f).

^{40}Mg, and ^{43}Al are just unbound (-250, -145, -470, and -550 keV, respectively). Experimentally the drip line has been probably reached for $Z=8$ (^{24}O) and for $Z=9$ (^{29}F). The last observed isotopes in the other chains are ^{32}Ne, ^{35}Na, ^{38}Mg, and ^{41}Al [17–23], and are very close to our predicted drip line.

B. Quadrupole properties and deformation

We have calculated the reduced transition probability $B(E2;2^+\rightarrow 0^+)$, the spectroscopic quadrupole moment Q_s, and the excitation energy of the first 2^+ state for all the even-even nuclei considered in this paper. Assuming that the rotational formula for the intrinsic quadrupole moment as a function of the $B(E2)$ is valid we get the values of the deformation parameter β using the expression

$$\beta = Q_0 \sqrt{\frac{5\pi}{3}}\, Z^{-1} R_0^{-2}.$$

The results for Ne and Mg are gathered in Table I. The results for the oxygen isotopes below the drip line are already known and nothing especially curious happens above it. Let us examine first the situation for the heavier isotopes, irrespective of the actual position of the drip line. For the neon isotopes we find a low-lying 2^+ in ^{32}Ne, ^{34}Ne, and ^{36}Ne, correlated with a strong $B(E2)(2^+\rightarrow 0^+)$ that should correspond to $\beta\approx 0.4$. At $N=28$—well beyond the drip line—our results show clearly the effect of the $N=28$ shell closure. The situation in the Mg isotopes is much richer. We observe in the table that the excitation energy of the 2^+ drops already at $N=22$ and stabilizes at around 1 MeV even for $N=28$. These $B(E2)$'s correspond to $\beta\approx 0.5$ for $N=24$ and $N=26$ and $\beta\approx 0.45$ for $N=28$ and $N=30$ and no shell closure effect is seen in this quantity either. Comparing with the Ne case we see that four active protons are required in order to break the $N=28$ shell closure. For six protons—Si isotopes—the shell closure is recovered because of the filling of the $1d_{5/2}$ orbit.

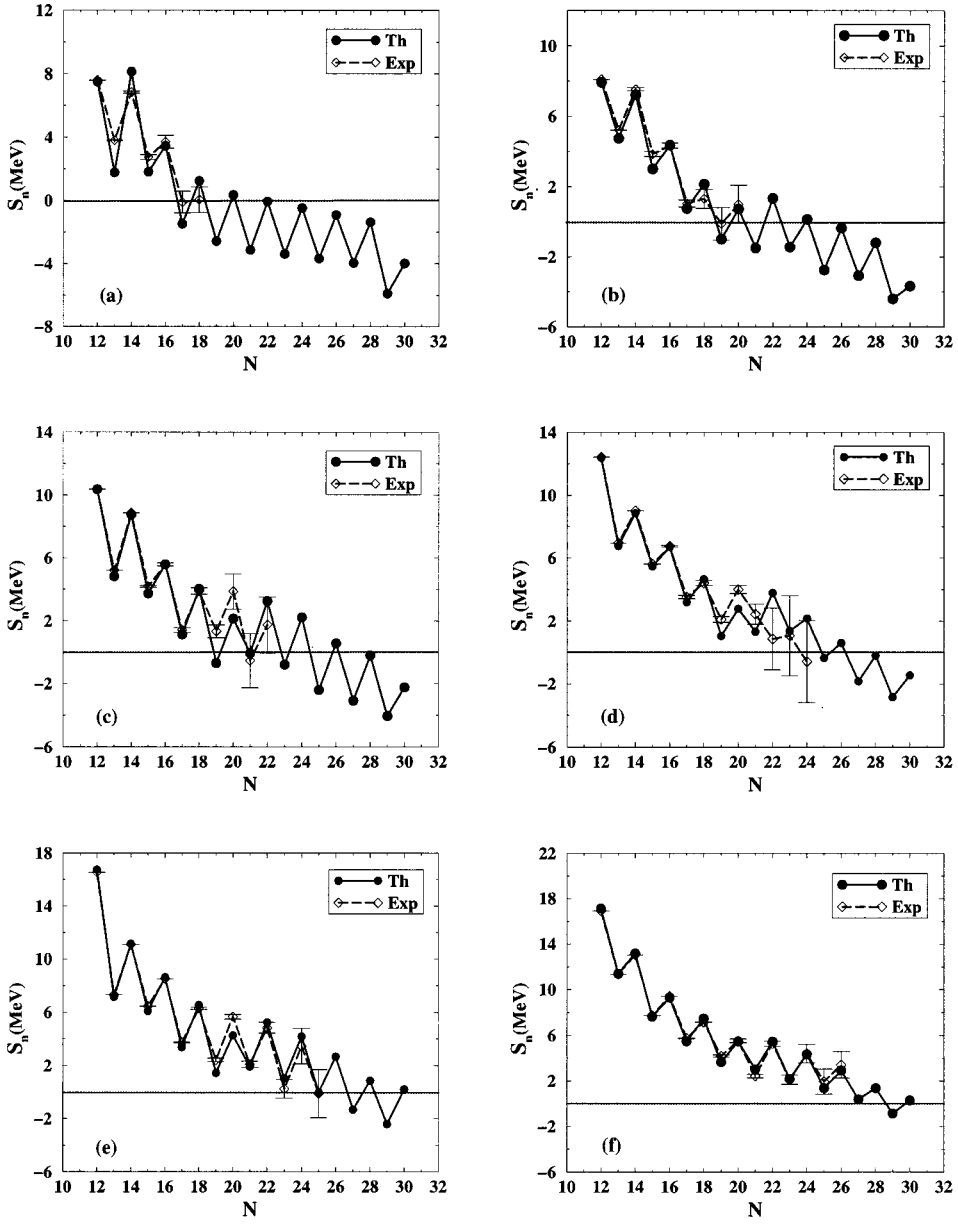

FIG. 2. Theoretical and experimental S_{1n} for O (a), F (b), Ne (c), Na (d), Mg (e), and Al (f).

TABLE I. $E2$ properties for the Mg and Ne nuclei. E_x in MeV, Q_s in e fm^2 and $B(E2)$ given in e^2 fm^4 units. Experimental values taken from Ref. [24].

N	Ne					Mg				
	$E_x(2^+)$		Q_s	$B(E2)$		$E_x(2^+)$		Q_s	$B(E2)$	
	Th	Exp	Th	Th	Exp	Th	Exp	Th	Th	Exp
14	2.18	1.98	−2.77	40.51	28	1.95	1.81	−11.73	65.97	61
16	2.03		−10.56	38.26		1.56	1.47	−15.67	60.65	68
18	1.83		−0.87	33.05		1.70	1.48	−11.57	48.34	
20	1.94		−1.02	23.41		1.71	0.89	−10.33	29.36	90
22	1.02		−11.16	51.49		1.21		−13.17	68.59	
24	0.90		−16.56	72.88		0.85		−19.29	94.69	
26	1.10		−14.30	61.38		0.93		−19.45	94.14	
28	1.98		0.97	52.02		1.05		−21.45	82.02	
30	1.26		−1.55	47.71		1.11		−13.48	83.35	

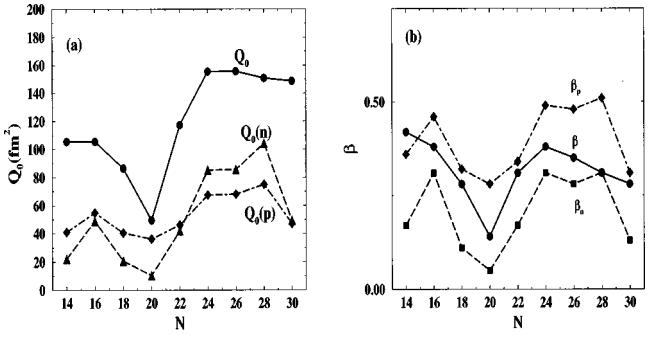

FIG. 3. Mass quadrupole properties of the magnesium isotopes.

In order to understand whether the large neutron excess may affect the proton and neutron deformations we have calculated the mass quadrupole properties. From them we get the intrinsic mass quadrupole moments and the corresponding $\beta_{\pi(\nu)}$ parameters. Figure 3 contains the mass quadrupole moments as well as those of neutrons and protons along the Mg isotope chain. Those of the neutrons are systematically larger than the proton ones, but this only reflects the fact that they are more abundant. In fact, when we normalize to the number of particles to obtain the β parameters [Fig. 3(b)], the situation is the opposite. This unexpected result stress the importance of the protons in keeping the deformation of the heavy magnesiums.

We have seen that the Mg isotopes are predicted to be deformed even for the magic neutron number $N=28$. We will examine now the structure of ^{40}Mg in more detail. In Fig. 4 we have plotted the occupation of the $1f_{7/2}$ neutron orbit from oxygen to silicon. Notice the dip at ^{40}Mg indicating that the $N=28$ closure is extremely weakened. In addition, the analysis of the structure of the wave function confirms that the closed shell configuration has lost its leading status because the configuration with two neutrons in the $2p_{3/2}$ orbit has equivalent weight (22 vs 28 %). Therefore, according to our calculation $N=28$ is not a closed shell at $Z=12$.

Now we come back to $N=20$. In the $0\hbar\omega$ valence space $N=20$ is closed by definition; this shows up in the rise of the 2^+ excitation energies and the decrease of the $E2$ transition probabilities. In ^{32}Mg both numbers have been measured and the discrepancies are huge; 1.71 MeV (th) vs 0.89 MeV (exp)

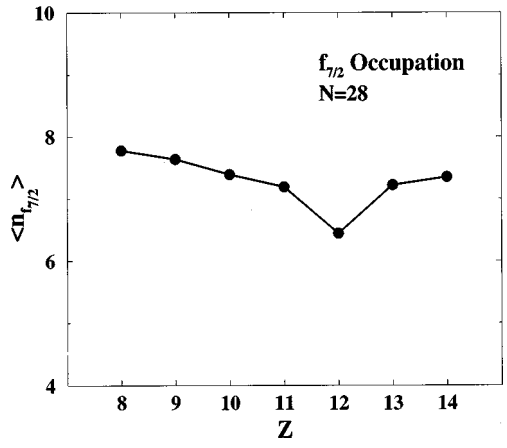

FIG. 4. Occupation of the $1f_{7/2}$ orbit in the $N=28$ isotones.

TABLE II. Weight of proton excitations in the intruder wave functions. Energies in MeV.

Nucleus	$(2p\text{-}2h)_\nu$		$(2p\text{-}2h)_{(\pi+\nu)}$		
	$E(0^+)$	n^ν_{pf}	$E(0^+)$	n^ν_{pf}	n^π_{pf}
^{30}Ne	−88.06	2	−88.09	1.93	0.07
^{32}Mg	−137.43	2	−137.48	1.95	0.05

[5] for the 2^+ energy and a predicted $B(E2)$ three times smaller than the measured value [7]. The body of evidence is convincing enough; if we assume that $N=20$ is closed we lose the necessary degrees of freedom to explain the behavior of the isotopes of Ne, Na, and Mg in the vicinity of the neutron number 20.

III. INTRUDER STATES AROUND $N=20$

A. Structure of the intruder states

In order to understand the behavior of the $N=20$ isotones far from stability an enlarged valence space has to be used. Several attempts have been already made as we mentioned in the Introduction. We are now able to deal with much larger dimensionalities using the code ANTOINE [25], and this makes it possible to improve our understanding of this problem. We will allow $2p\text{-}2h$ neutron jumps from the sd to the pf shell and argue that these are the main components of the physical states. First we can gather from Table II that the influence of the proton excitations across $N=20$ is negligible.

Another issue is whether intruders are dominated by $2p\text{-}2h$ or $4p\text{-}4h$ excitations. The larger the number of jumps the larger the dimensionality. For this reason we have truncated the pf shell to only the $1f_{7/2}$ and the $2p_{3/2}$ subshells. We have calculated the first $2p\text{-}2h$ and $4p\text{-}4h$ 0^+ states for ^{32}Mg. Their energies are −136.48 and −129.23 MeV, respectively. The difference is large enough to be sure that even if the full pf shell were taken into account, the $4p\text{-}4h$ excitations will not dominate. To sum up, the intruders around $N=20$ far from the stability are built by two neutron excitations from the sd to the pf shell. The next task is to define the borders of the region where these states become dominant in the ground state wave functions.

B. The island of inversion

In order to accomplish this task we have undertaken a systematic calculation of the energy gap between normal and intruder states in for $8\leqslant Z\leqslant 14$, $18\leqslant N\leqslant 22$. Table III and Fig. 5 show that there are very few nuclei where the inver-

TABLE III. Intruder gap in MeV.

N	O	F	Ne	Na	Mg	Al	Si
18	5.79	4.95	2.99	2.75	3.19	4.67	5.50
19	4.15	2.91	0.85	0.83	1.01	2.98	3.35
20	2.54	1.04	−1.04	−1.07	−1.05	0.82	1.80
21	3.87	2.63	−0.03	−0.80	−0.10	1.91	2.96
22	4.86	3.52	1.78	1.27	1.38		

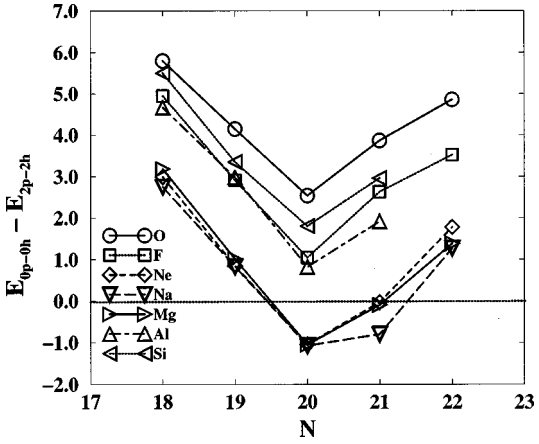

FIG. 5. $2p$-$2h$ gap for the different isotopic series.

sion of configurations takes place. Only ^{30}Ne, ^{31,32}Na, and ^{32}Mg are dominated by the $2p$-$2h$ states. Moreover, normal and intruder states are almost degenerate in ^{31}Ne and ^{33}Mg. However, the experiments seem to indicate that at $N=19$ the intruders and the normal state are closer than we predict. It may well happen that our interaction places the intruders a few hundred keV too high. Anyhow, even if we decrease by 1 MeV the intruder gap, the anomalous region is still constrained to $10\leqslant Z\leqslant 12$, $19\leqslant N\leqslant 22$ with both types of states almost degenerate at $N=19$ and $N=22$. Notice that in this case the gains in energy of the intruders will solve the anomalies in the separation energies discussed in Sec. II. Moreover, a small intruder mixing in the ground state of ^{29}F will lead to an energy gain of a few hundred keV, enough to bind it, therefore restoring the agreement with the experimental situation.

The inversion of configurations results of the competition of the monopole field, that favors the normal filling and the correlations that favors open shell intruders. To study their interplay, we have decomposed the gap in two parts: the monopole gap and the contribution of correlations, i.e., the multipole gap. Let us consider the monopole energy of the normal and $2p$-$2h$ intruder 0^+ states. The differences give us the monopole gap, essentially related to the single particle gap. The results for the Mg isotopes are shown in Fig. 6(a). The minimum is reached at $N=20$ and it increases as we add neutrons to the pf shell. On the contrary, the behavior of the correlation energy is rather different. We shall compute the correlation energies in the truncated space mentioned in Sec. III A. It can be seen in Fig. 6(b) that, as expected, the intruders are more correlated than the corresponding $0\hbar\omega$ states. However, the difference in correlation energy decreases as the number of neutrons increases. Therefore, excitations of two neutrons from the sd shell to the pf shell become rapidly unfavored when $N\neq 20$.

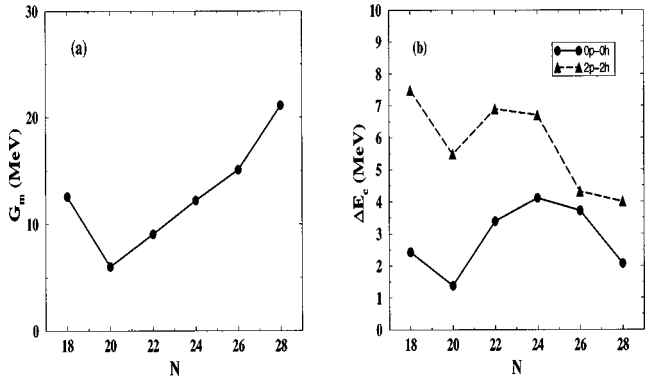

FIG. 6. Monopole gaps and correlation energies for the magnesium isotopes.

C. Some properties of the intruders

The intruders dominate the ground states of ^{30}Ne, ^{31}Na, and ^{32}Mg. At $N=21$ (^{31}Ne, ^{32}Na, and ^{33}Mg) they are nearly degenerate with the closed shell states—actually they are also degenerate with the positive parity $1p$-$1h$ intruders—which makes it extremely difficult—if not plainly impossible—to advance any sound prediction. Thus, we shall in what follows limit ourselves to discuss some of the properties of the $N=20$ intruders that, although eroded by the mixing with the closed shell, will certainly be a very good approximation to those of the physical states.

^{30}Ne. The excitation energy of the 2^+ is 0.93 MeV and the $B(E2)\uparrow$ is 370 e^2 fm^4 which corresponds to a deformation $\beta\approx 0.4$.

^{31}Na. The intruder bandhead is a $3/2^+$ which restores the agreement with the measured value of the ground state angular momentum. The deformation assuming $K=3/2$ is $\beta\approx 0.45$. The excited $5/2^+$ is located at 200 keV of excitation energy. The experimental magnetic moment is $2.28\mu_N$ [26]. The intruder's value, $2.19\mu_N$, is in better agreement with this value than the closed shell value for the $3/2^+$ state, $2.50\mu_N$. Our value is very close to the prediction given in [13] using a smaller valence space. Notice also that the mixing between the intruder and the normal state will increase the value of μ moving it towards the experimental number.

^{32}Mg. The 2^+ excitation energy is 1.03 MeV compared with the experimental value 0.89 MeV. The $B(E2)\uparrow$, 490 e^2 fm^4, also fits nicely with the experimental value 450 e^2 fm^4. It corresponds to a deformation $\beta\approx 0.5$. We have computed as well the $BE2\uparrow$ from the ground state of the $4p$-$4h$ configuration to its first excited 2^+ and we find 650 e^2 fm^4 which is much bigger than the experimental number. Moreover, the increase in $BE2$ from the closed shell to the $2p$-$2h$ intruder (340 e^2 fm^4) is larger than the one from $2p$-$2h$ to $4p$-$4h$ (160 e^2 fm^4). As the gain in quadrupole energy is roughly proportional to the $BE2$ value, we understand why the $4p$-$4h$ configuration is higher in energy than the $2p$-$2h$ one.

In Fig. 7(a) we compare the experimental excitation energy of the 2^+ states with the theoretical predictions along the Mg chain. In fact we shall use the predictions obtained in the $0\hbar\omega$ or the $2p$-$2h$ spaces depending on whether the ground-state is a normal or an intruder state. The agreement is extremely good. This is also the case for the $E2$ reduced transition probabilities shown in Fig. 7(b). In these figures a small kink appears at $N=22$, however, it can be smoothed or even disappear if we take into account the mixing with the—very collective—$4p$-$2h$ intruder. Therefore, our prediction for the $B(E2)$ and the 2^+ excitation energy of ^{34}Mg would rather be somewhere in between the interpolation of the ^{32}Mg and ^{36}Mg points in Fig. 7(b) and the actual ^{34}Mg points.

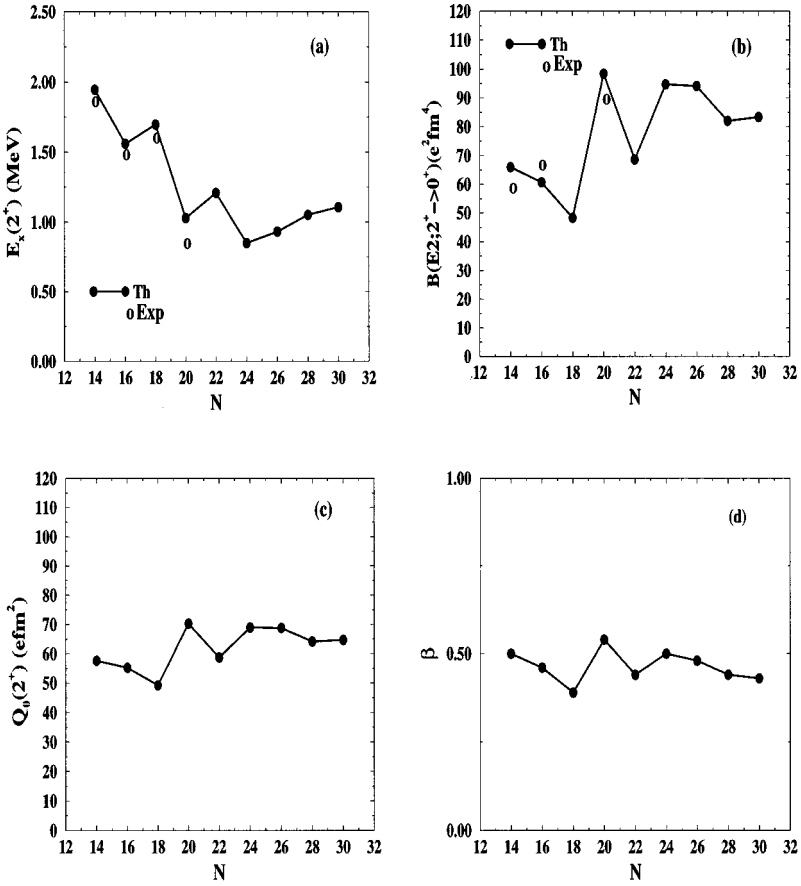

FIG. 7. $E2$ properties of the magnesium isotopes.

From the $B(E2)$ values we can get some insight into the structure of the intrinsic states. This can be achieved calculating the values of the intrinsic quadrupole moment and the deformation parameter β. Figures 6(c) and 6(d) plot these quantities. We see that the deformation is quite constant along all the chain.

IV. THE MIXING BETWEEN NORMAL AND INTRUDER STATES IN ^{34}Si

The mixing of the intruders and the closed shell states to build the physical wave functions is a very delicate issue; first, because our effective interaction was tailored for a valence space that did not contain the intruder's degrees of freedom, therefore incorporating in some measure their effect. Secondly because we are not able yet to perform a full and consistent calculation including all the np-nh intruders. Nevertheless, and with these caveats, we will explore below this issue in a nucleus, ^{34}Si that lies outside the island of inversion.

In ^{34}Si, the ''unmixed'' situation is the following. The first $2p$-$2h$ 0^+ state lies at 1.7 MeV excitation energy with respect to the $0p$-$0h$ 0^+ ground state. The 2^+ states lie respectively at 3.0 MeV ($2p$-$2h$) and 4.9 ($0p0h$) MeV. These values are compatible with the experimental energies. However, within this picture, the probability for the transition $2_1^+ \rightarrow 0_1^+$ vanishes, contrary to the experimental situation. To get a mixed solution we first diagonalize separately the Hamiltonian in the $0p$-$0h$ and the $2p$-$2h$ spaces. Then we take the lowest eigenstate in each space and rediagonalize in the basis spanned by these pairs of states. The results are shown in Table IV, where we give the percentages of $0\hbar\omega$ components in the different states, the excitation energies, and the transition probabilities, compared with the experimental results and with other shell model calculations. In

TABLE IV. ^{34}Si excitation energies (in MeV) and transition probabilities in e^2 fm^4.

J^π	$0\hbar\omega$	ΔE				$B(E2\uparrow)$				
	%	this work	[28]	[13]	exp.		this work	[28]	[13]	exp.
0_1^+	80	0.0	0.0	0.0	0.0	$0_1^+ \rightarrow 2_1^+$	147	44	180	85(33)
0_2^+	20	3.0	2.0	2.0		$0_1^+ \rightarrow 2_2^+$	78	108		<104
2_1^+	6	3.5	2.8	2.0	3.3	$0_2^+ \rightarrow 2_1^+$	260	215		
2_2^+	94	5.6	4.9	4.1						

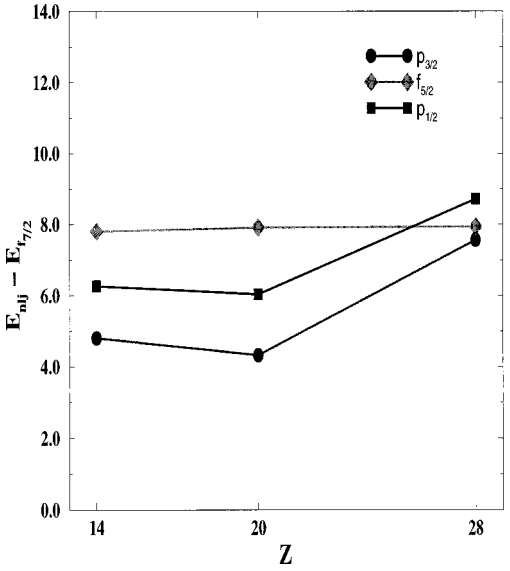

FIG. 8. Single-particle energies along $N=28$.

addition to the data of Ref. [27], we include the new coulex results [28] that give us access to the quadrupole properties of ^{34}Si.

Our calculation is in full agreement with the experimental results. In the shell model study included in Ref. [28], made in a valence space more truncated than ours, the first excited state of ^{34}Si is also predicted to be a 0^+ even if located at a smaller excitation energy. Both calculations give qualitatively the same picture although our numbers are closer to the experimental ones. In Ref. [13] another shell model calculation in a smaller valence space is made, that gives a more compressed spectrum, with a too low first excited 2^+ state. A remarkable aspect—common to the three calculations available—is that the ground state of ^{34}Si has $0p$-$0h$ nature while its two lowest excited states are intruders (see Table IV). This is a feature characteristic of double magic nuclei, ^{40}Ca, for example, and suggests that ^{34}Si could actually be considered as such.

V. COMPARISON WITH MEAN FIELD CALCULATIONS

The aim of this section is to compare our results with those obtained by several authors using the Hartree-Fock Bogolyubov framework. Dobaczeswski *et al.* [29] have included to a large extent the effects of the continuum working in the cordinate space. As the neutron excess increases the single particle potential becomes shallower and the densities expand into a larger region. This is particularly true for the outermost neutrons characterized by long-tail wave functions. The corresponding quasi-particle levels spread uniformly without strong shell gaps. In the pf shell the $f_{7/2}$-$p_{3/2}$ gap is eroded when compared to its value near the stability.

In our context, the evolution of the effective single particle energies is governed by the monopole part of the interaction. When $2\hbar\omega$ excitations are excluded (as in almost every shell-model calculations) the monopole gives rise to a linear evolution of the single particle spectrum between two subshell closures. Figure 8 shows the evolution of the single-particle energies for $N=28$ predicted in our model. At $N=Z=28$ there is a strong gap between the $f_{7/2}$ and the remaining orbits which fall in a rather small energy range. When the number of protons reduces to $Z=20$ there is a clear erosion of the $f_{7/2}$-$p_{3/2}$ gap while the other two gaps undergo a smooth increase. Moreover the $f_{5/2}$ and $p_{1/2}$ orbits come out interchanged. The spectrum remains stable as Z decreases to 14. The $N=28$ shell gap becomes smaller and the general pattern of the spectrum is more uniform approaching that of a well with a very diffuse surface [29].

Terasaki *et al.* [30] have studied the quadrupole properties of the Mg isotopes from the stability to the drip lines. Many of our main conclusions agree with their outcomes. Both approaches place the neutron drip line around ^{40}Mg. The three isotopes ^{36}Mg, ^{38}Mg, and ^{40}Mg are found to be strongly deformed. In our work the total mass quadrupole moments of these nuclei are close to 160 fm^2, while their values are slightly higher, going from 175 to 200 fm^2. The agreement becomes extensive to the individual behavior of protons and neutrons. Actually, it is found in the two descriptions that protons become a bit more deformed than neutrons. However, they cannot explain the onset of deformation at $N=20$ a feature also present in the calculations that use the Gogny force [31]. The energy vs deformation curves produced by calculations are very similar, they present a spherical minimum and a shoulder at $\beta=0.5$. It is only when the Bohr Hamiltonian is solved in the (β,γ) plane that a deformed ground state is obtained, a calculation only available for the Gogny force [31]. A more detailed comparison between the shell model and mean field results is in progress. Let us finally mention that the relativistic mean field calculations of Ref. [32] place the drip line at values of N much larger than the nonrelativistic ones and than ours. This is related to the behavior of their gap that becomes essentially zero, leading to very small but positive separation energies.

VI. CONCLUSIONS

In this work we have shown that the spherical shell model description can be successfully applied to nuclei very far from stability, using the same effective interaction and the same valence space one should use for the stable isotopes. This is a very satisfactory result that enhances our confidence in the predictive power of our model. In the region we have chosen to study, the collective behavior is of overwhelming importance and—another satisfying aspect—can be dealt with in a spherical approach. The magnesium isotopes behave in a rather iconoclastic way. For, in the two cases they have a magic neutron number they manage to break it. At $N=20$ this is due to the inversion of the closed neutron shell configuration and the intruder ones (deformed $2p$-$2h$ neutron jumps from the sd shell to the pf shell). At $N=28$ the quadrupole correlations at $0\hbar\omega$ are responsible for the disappearance of the neutron magicity.

ACKNOWLEDGMENTS

We thank G. Walter and A. Zuker for many discussions. This work was partially supported by the IN2P3 (France) CICYT (Spain) agreements and by DGES (Spain) Grant Nos. PB96-53 and PB96-604.

[1] J. Retamosa, E. Caurier, F. Nowacki, and A. Poves, Phys. Rev. C **55**, 1266 (1997).
[2] T. R. Werner, J. A. Sheikh, W. Nazarewicz, M. R. Strayer, A. S. Umar, and M. Misu, Phys. Lett. B **335**, 259 (1994).
[3] C. Thibault *et al.*, Phys. Rev. C **12**, 193 (1975).
[4] C. Detraz, D. Guillemaud, G. Huber, R. Klapisch, M. Langevin, F. Naulin, C. Thibault, L. C. Carraz, and F. Touchard, Phys. Rev. C **19**, 171 (1979).
[5] D. Guillemaud, C. Detraz, M. Langevin, F. Naulin, M. de Saint-Simon, C. Thibault, F. Touchard, and M. Epherre, Nucl. Phys. **A246**, 37 (1984).
[6] G. Klotz *et al.*, Phys. Rev. C **47**, 2502 (1993).
[7] T. Motobayashi *et al.*, Phys. Lett. B **346**, 9 (1995).
[8] X. Campi, H. Flocard, A. K. Kerman, and S. Koonin, Nucl. Phys. **A251**, 193 (1975).
[9] B. H. Wildenthal, M. S. Curtin, and B. A. Brown, Phys. Rev. C **28**, 1343 (1983).
[10] A. Poves and J. Retamosa, Phys. Lett. B **184**, 311 (1987); Nucl. Phys. **A571**, 221 (1994).
[11] E. K. Warburton, J. A. Becker, and B. A. Brown, Phys. Rev. C **41**, 1147 (1990).
[12] N. Fukunishi, T. Otsuka, and T. Sebe, Phys. Lett. B **296**, 279 (1992).
[13] T. Otsuka and N. Fukunishi, Phys. Rep. **264**, 297 (1996).
[14] B. H. Wildenthal, Prog. Part. Nucl. Phys. **11**, 5 (1984).
[15] A. Poves and A. Zuker, Phys. Rep. **70**, 4 (1981).
[16] O. Tarasov *et al.*, Phys. Lett. B **409**, 64 (1997).
[17] D. Guillemaud-Mueller *et al.*, Z. Phys. A **332**, 189 (1989).
[18] D. Guillemaud-Mueller *et al.*, Phys. Rev. C **41**, 937 (1990).
[19] M. Langevin *et al.*, Phys. Lett. **125B**, 116 (1983).
[20] N. A. Orr, W. Mittig, L. K. Fifield, M. Lewitiwicz, E. Plagnol, Y. Schutz, Zhan Weng Long, L. Bianchi, A. Gillibert, A. V. Belozyorov, S. M. Lukyanov, Yu. E. Penionhkevich, A. C. C. Villari, A. Cunsolo, A. Foti, G. Audi, C. Stephan, and L. Tasson-Got, Phys. Lett. B **258**, 29 (1991).
[21] X. G. Zhou, X. L. Tu, D. J. Vieira, K. E. G. Löbner, H. L. Seifert, Z. Y. Zhou, and G. W. Butler, Phys. Lett. B **260**, 286 (1991).
[22] H. Sakurai *et al.*, Nucl. Phys. **A616**, 331c (1997).
[23] G. Audi, O. Bersillon, J. Blanchot, and A. H. Wapstra, Nucl. Phys. **A624**, 1 (1997).
[24] S. Raman, C. W. Nestor, S. Kahane, and K. H. Bhatt, At. Data Nucl. Data Tables **42**, 1 (1991).
[25] E. Caurier, code ANTOINE, Strasbourg, 1989.
[26] G. Huber *et al.*, Phys. Rev. C **18**, 2342 (1978).
[27] P. Baumann *et al.*, Phys. Lett. B **228**, 458 (1989).
[28] R. W. Ibbotson *et al.*, Phys. Rev. Lett. **80**, 2081 (1998).
[29] J. Dobaczeswki, W. Nazarewicz, T. R. Werner, J. F. Berger, C. R. Chinn, and J. Decharge, Phys. Rev. C **53**, 2809 (1996).
[30] J. Terasaki, H. Flocard, P. H. Heenen, and P. Bonche, Nucl. Phys. **A621**, 706 (1997).
[31] M. Girod and S. Peru (private communication).
[32] G. A. Lalazissis, D. Vretenar, W. Pöschl, and P. Ring, Nucl. Phys. **A632**, 363 (1998).